Effect of Deep Penetration of Interleaf on Delamination Resistance in GFRP

Dakai Bian[1]
Department of Mechanical Engineering,
Columbia University,
New York, NY 10027
e-mail: db2875@columbia.edu

Tizian Bucher
Department of Mechanical Engineering,
Columbia University,
New York, NY 10027

D. J. Shim
GE Global Research,
Niskayuna, NY 12309

Marshall Jones
GE Global Research,
Niskayuna, NY 12309

Y. Lawrence Yao
Department of Mechanical Engineering,
Columbia University,
New York, NY 10027

The problem of improving the delamination resistance and toughness of laminate fiber-reinforced composites especially for the drop-off structure is receiving considerable attention with the increasing need and application in industries. A hot melt-bonding process is developed to bond glass fabric laminates and the thermoplastic (TP) polysulfone (PSU) interleaf prior to the vacuum assisted resin transfer molding (VARTM) of laminate composites. The TP interleaf is heated above the glass transition temperature to reduce the viscosity when penetrating deeply into the glass fiber fabric. Mechanical tensile testing is performed to quantify the effects of the penetration depth on composite delamination resistance and composite toughness under different melt-bonding temperatures. Crack paths are observed by optical microscopy to characterize the crack propagation and arrest mechanism. Postmortem high-resolution imaging of the fracture surfaces is used to characterize the toughening mechanism of the TP interleaf reinforcements by using scanning electron microscopy (SEM). With deep penetration of the interleaf into the fiber bundles, cracks arrested within the penetration region improve the toughness by avoiding the cracks to reach the weak interface between interleaf and epoxy.
[DOI: 10.1115/1.4032566]

Keywords: deep penetration, delamination, toughening, crack path, thermoplastic interleaf

1 Introduction

Fiber-reinforced polymer (FRP) composites have been widely used. The applications of the composites span automotive, marine, and aerospace industries. These industries are dedicated to increase the use of FRP in their products in an effort to decrease weight and increase energy efficiency.

As glass fiber-reinforced polymer (GFRP) is often used as laminated structures, the composites are prone to delamination when loaded due to their poor through thickness strength. For some specific product structures like turbine blades, the tapered shape leads to stress concentration at the areas where there is a drop-off laminar, causing catastrophic failure. Efforts have been made to improve the fracture toughness and delamination resistance of GFRP structures, especially the ones involving drop-offs.

Some researchers strived to improve the delamination resistance and toughness by increasing the ductility of the entire matrix. From the research of Leach and Moore [1], the TP matrix, polyether ether ketone (PEEK), significantly increases the delamination resistance and toughness; however, the major disadvantage of carbon fiber (CF)/PEEK is also obvious; it requires high temperature and pressure during the molding process due to the higher viscosity of TPs, and thus increases the cost and implementation difficulties [2]. Some other researchers [3] enhance the composites toughness by improving the design of composite structures, such as "feathering," which includes extending alternating laminates beyond the ply-drop to decrease the severity of the drop-off layer, as well as "*z*-spiking," in which the stitches of the drop-off layer are removed and the fiber bundles are directly driven into the fiber bundles of the adjacent core layer, the delamination resistance increased; however, it is not easy to control the distance between drop-offs during fabrication procedure and may disrupt the fiber structure and create resin-rich zones.

Another method is to locally toughen the composites and modify the resin-rich layer in between the plies, known as interleaving, in which a ductile material is inserted between the plies. From the research of Ozdil and Carlsson [4], the tested TP interleaved composites showed that the low adhesion between the interleaf material and the matrix caused the poor interface adhesion and toughness. The results indicate that both high toughness and adhesion strength are required for the interleaf material. Many approaches have been attempted to achieve this purpose, such as incorporating nylon particles [5], modified powder/spray tackifier [6], nanofibers [7–10], and TP/CF veil [11], but the adhesive failure between the interleaf and matrix still remains. One of the new approaches taken by Hojo et al. [12–14] involves a new type of TP, ionomer, which is a polymer partially ionized by the metallic ion, used as interleaf. Because of its active chemical property, it has good adhesion to epoxy resin that creates a thin layer, which is a mixture of fiber, resin, and ionomer. In this case, the matrix and interleaf have higher bonding strength; when a crack propagates, it needs more energy to go through the plies. However, the thickness of the mixed zone is only around one to two fiber diameters, and the plastic zone ahead of the crack can still reach the interface between the interleaf and epoxy, and thus limit the fracture toughness improvement. If a TP interleaf penetrates much deeper into the fiber bundles, such a plastic zone ahead of a crack is more likely to remain within the penetrated region without reaching the interface of the interleaf material and epoxy and as a result, more fracture energy is required for delamination to occur.

In the present study, a hot melt-bonding process of a TP interleaf is investigated. The relationship between the bonding temperature and the penetration depth of the interleaf into fiber bundles was investigated. Interlaminar mixed-mode fracture properties of the interleaved GFRP were studied as a function of the penetration depth. The dependence of crack path and propagation behavior as well as crack arrest and toughening mechanism on the penetration depth was investigated and discussed.

[1]Corresponding author.
Manuscript received May 30, 2015; final manuscript received November 7, 2015; published online March 10, 2016. Assoc. Editor: Donggang Yao.

2 Background

2.1 Loading Conditions at the Drop-Off Structure. GFRPs are widely used due to their high strength, light weight, and low cost. One of the important applications is the wind turbine blade. In service, the blade is subjected to complex loadings induced by the turbine rotation and variable wind loadings [15]. The loads in the flapwise direction and centrifugal forces are two important factors that may lead to failure of the blade, as indicated by arrows in Fig. 1(*a*). Due to aerodynamic requirements and weight constraints, geometric properties are required to vary along the length of the wind turbine blade, and ply drop-offs are introduced by piling up hundreds of plies at the root but only a few at the tip (Fig. 1(*a*)). The drop-off plies cannot carry any load at the termination location, and thus, the far-field load carried by the drop-off plies needs to be transferred to the adjacent continuous plies via interlaminar stresses [17]. An interleaf is also shown at the drop-off site.

Free-body diagrams of the external drop-off layer and the interleaf are shown in Figs. 1(*b*) and 1(*c*). The applied loads can be either in-plane or bending loads or both. As required by the force equilibrium on the drop-off structure, the interlaminar shear stress must exist along the lower surface, equal to and opposite to the net far-field loads. Normal stress exists due to the moment equilibrium about point O and its integral along *x*-direction equal to and opposite to the applied load in the *z*-direction. The free-body diagram of the thin interleaf beneath the drop-off ply is determined the same way.

The drop-off structure has the following force distribution. The peak interlaminar normal stress is at the terminated surface, and the peak interlaminar shear stress occurs slightly before the terminated surface and shrinks to zero at the terminated surface both under in-plane loads and bending loads [17,18] and illustrated in Fig. 2(*a*). The corresponding interlaminar stress distribution on the interleaf is determined by the principle of action and reaction.

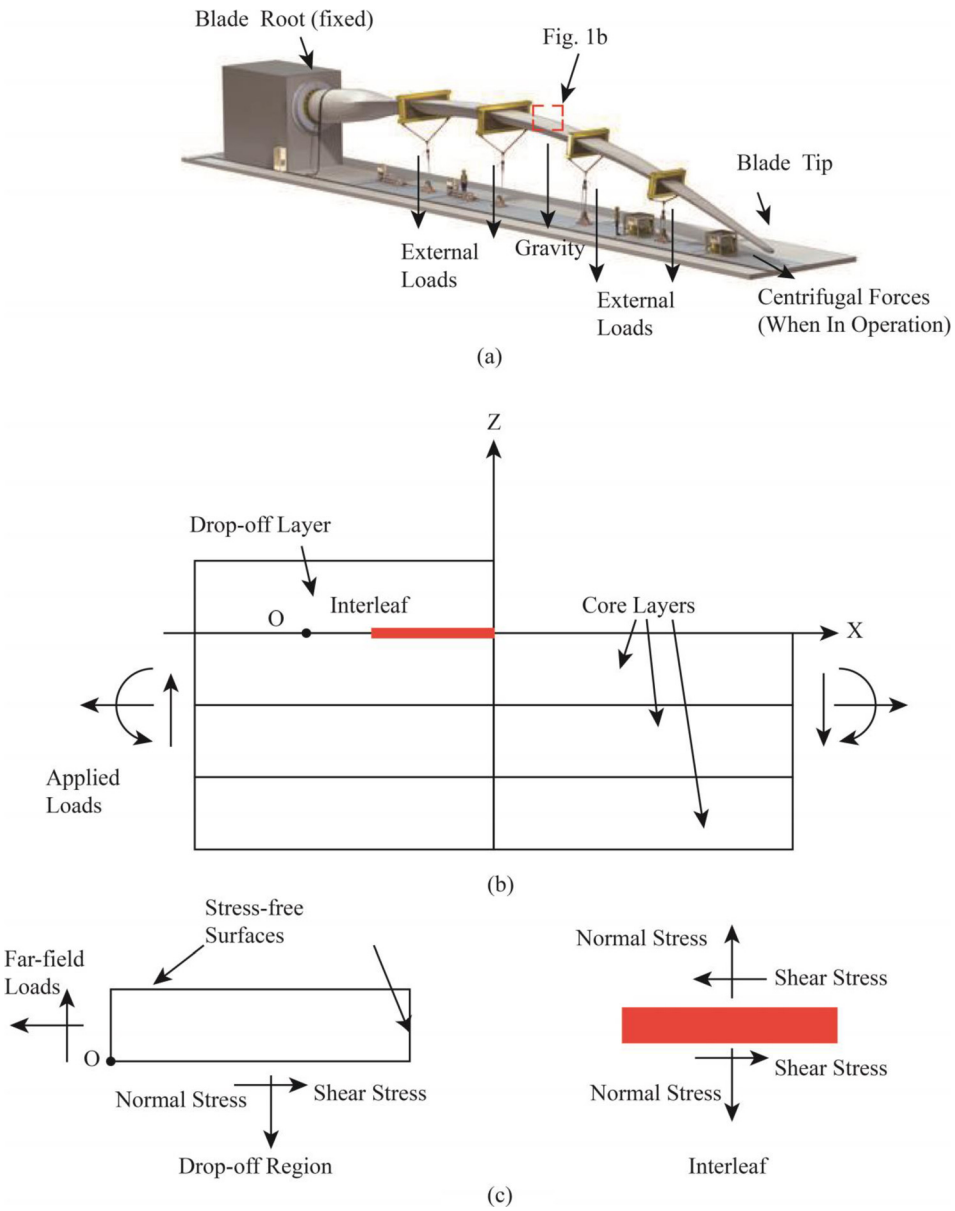

Fig. 1 (*a*) MTS System Corporation used their special testing system to test the wind turbine blade to failure under the flapwise loads. When the blade is in operation, the centrifugal forces will occur due to turbine rotation [16]. (*b*) Schematic of the specimen under external loads: interleaf is inserted between the external drop-off layer and the core layers. (*c*) Free-body diagrams of the drop-off region and interleaf: applied force and moment equilibrium about point O, both normal and shear stresses exist in the drop-off region and interleaf.

It is observed that the peak interlaminar stress can be reduced significantly by inserting an interleaf of lower stiffness, and the interlaminar stress is relieved if a tough interleaf is presented to undergo the necessary plastic deformation, which helps to absorb more incident energy [19].

2.2 Crack Initiation and Propagation. By using quadratic stress criterion for initiation of delamination [20]

$$\left(\frac{\sigma_s}{Z_s}\right)^2 + \left(\frac{\sigma_n}{Z_n}\right)^2 > 1 \tag{1}$$

where σ_s is the interlaminar shear stress, Z_s is the interlaminar shear strength, σ_n is the interlaminar normal stress, and Z_n is the interlaminar normal strength; the crack will initiate near point A or point C (Fig. 2(*b*)), which means that the crack is more likely to initiate at the interfaces. Under the in-plane loading condition, for the external drop-off ply, the crack is influenced by both mode I (opening) and mode II (shear) fracture. After the crack initiates, it propagates essentially in the weakest region within the crack tip plastic zone [21]. For the brittle materials with high yield strength, near the tip, the stress reaches the ideal strength, which is large enough to break the bond and allow the crack to spread. For more ductile materials, the stress still rises as the crack tip is approached, but when it exceeds the yield strength, the materials yield, and then a plastic zone forms at the crack tip and relieves the stress.

The main purpose of inserting a TP interleaf into the resin-rich zone is to toughen this brittle region and increase the delamination resistance by absorbing more energy when crack propagates. However, due to the low bonding energy between the interleaf material and epoxy, the crack tip plastic zone can still reach this interface and propagate along it even if the interleaf migrates a little (one to two fiber diameters) into the matrix as ionomer described in Sec. 1 (Fig. 3(*a*)). Thus, the hot melt-bonding method is introduced to increase the penetration depth. It is believed that with deeper penetration (five to six fiber diameters) of the interleaf

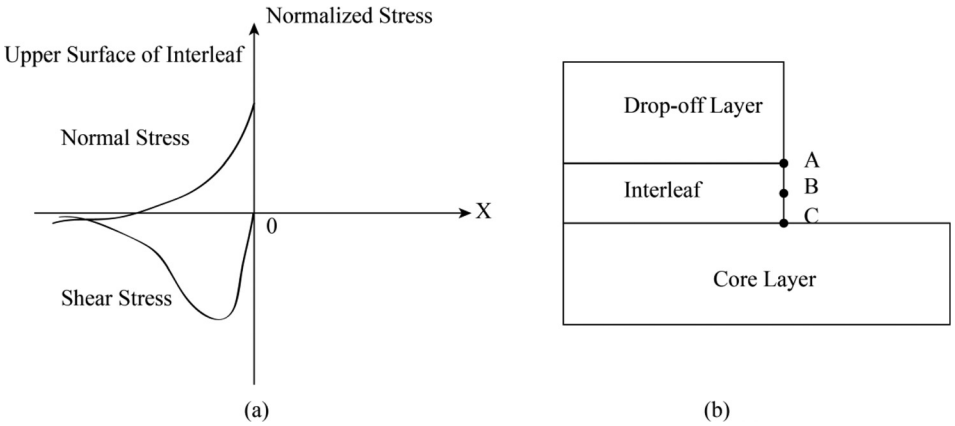

Fig. 2 (*a*) Illustration of the interlaminar shear and normal stress distribution along *X*-direction on the upper surface of the interleaf: the trends of the shear stress and normal stress are based on the analysis of the force and moment equilibrium for the external drop-off layer [18]. For the lower surface of the interleaf, the stresses are of the same magnitudes but opposite directions. Peak stresses occur close to the terminated surface. (*b*) Considering both normal and shear interlaminar stresses near or on the terminated surface of the interleaf, a crack is more likely to initiate near points A and C.

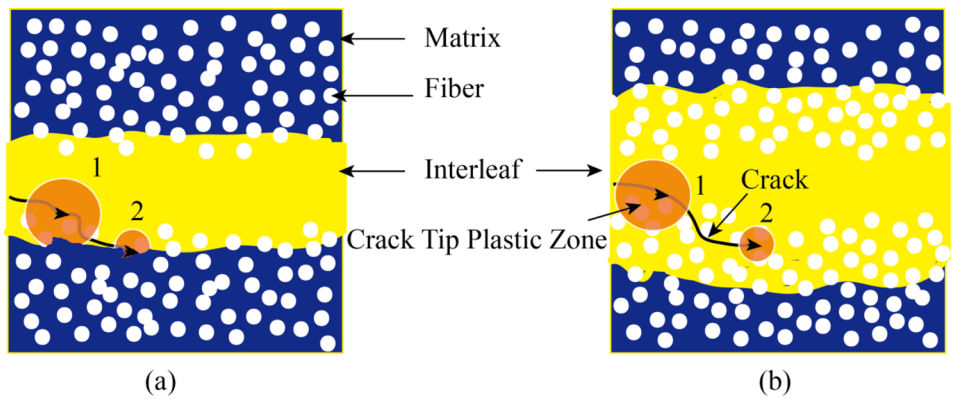

Fig. 3 (*a*) Schematic of the crack path under low penetration condition: crack initiates near the boundary of the pure interleaf region and the large plastic zone ahead of the crack tip reaches the interface between interleaf/fiber and epoxy/fiber, indicating that the crack migrates to this weak interface from point 1 to point 2 with the decreasing plastic zone size due to the rigid fiber. (*b*) Schematic of the crack path under high penetration condition: After crack initiates, the plastic zone only reaches the mixed region of interleaf and fiber (point 1). The decreasing plastic zone size arrests the crack propagating in the middle of the mixed region (point 2), where the delamination resistance is much larger than the interface between interleaf/fiber and epoxy/fiber.

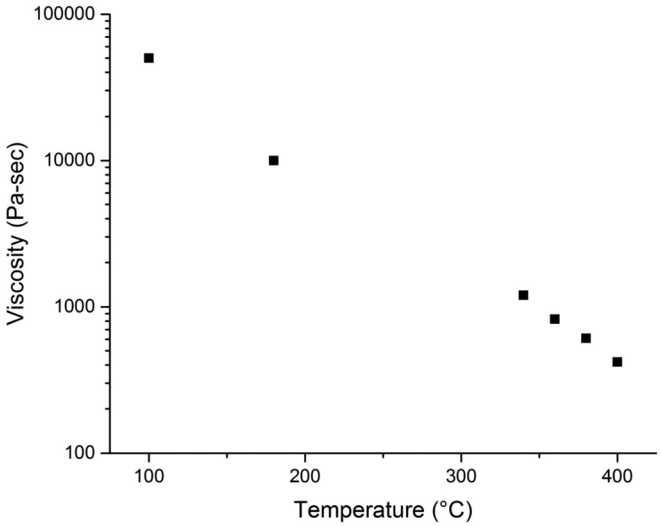

Fig. 4 PSU viscosity versus temperature [23]

into the fiber bundles, the plastic zone ahead of the crack tip is more likely to remain within the penetrated zone, and thus not reach the interface between interleaf and epoxy; as a result, the crack propagates within the penetration region and consumes more fracture energy (Fig. 3(*b*)).

2.3 Viscosity Effect and Interleaf Flow Analysis. It is believed that melt bonding leads to a deeper interleaf penetration into the fiber bundles, which can keep the crack inside of the mixed zone. The heating temperature is increased above the glass transition temperature of the TP interleaf material to soften the interleaf, decreasing the viscosity and thus facilitating its flow into the fiber bundles. Due to the fact that the heating temperatures are much higher than the glass transition temperature of the TP, the temperature-dependent viscosity η of the TP material can be modeled by a modified Arrhenius equation with glass transition temperature T_g as shown below [22]:

$$\eta(T) = A \exp\left(\frac{B}{T - T_g}\right) \tag{2}$$

When heated above the glass transition temperature, the viscosity will rapidly decrease. In this case, the temperature-dependent viscosity of PSU is shown in Fig. 4 [23].

With the above knowledge, a model to predict the penetration depth is developed. The fiber fabric is considered as a porous flat plate with rectangular channels evenly distributed along the surface. An interleaf is pressed with an externally applied pressure and the only movement is in the penetration direction (z-direction). Further assuming that the interleaf undergoes incompressible creeping flow and from Poiseuille's law, the average velocity through the section of the interleaf, which has not penetrated into the porous structure in z-direction yet, is

$$-\frac{dz_i}{dt} = \frac{L^2}{12 \times \eta} \times \frac{P - P_1}{z_i} \tag{3}$$

where z_i is the thickness of the interleaf not penetrating into the fabric yet, L is the length of the interleaf, η is the flow viscosity, P is the pressure on the thin interleaf in z-direction, and P_1 is the pressure on the interface between the interleaf and porous structure. The average velocity of the penetrated interleaf along the channels in the porous structure in z-direction is

$$\frac{dz_p}{dt} = \frac{d^2 \times P_1}{12 \times \eta \times z_p} \tag{4}$$

where z_p is the penetration depth and d is the width of the above-mentioned rectangular channels.

From mass conservation, the reduction of interleaf equals the amount of interleaf that penetrates into the porous structure

$$-\frac{dz_i}{dt} \times L = \frac{dz_p}{dt} \times (1 - f) \times L \tag{5}$$

where f is the fiber volume fraction.

By rearranging the above equations and integrating, the final penetration depth is

$$\frac{1}{2}\left\{z_o^2 - \left[z_0 + (f - 1) \times z_p\right]^2\right\} = \frac{t \times L^2 \times P_a}{12 \times \eta}\left\{1 - (1 - f) \times \frac{z_p}{z_0}\right\} - \frac{L^2 \times z_p^2}{2 \times d^2} \tag{6}$$

where z_0 is the original thickness of the interleaf, t is dwell time, and P_a is the applied pressure from clamps.

3 Experiment Procedures

The main objective of the experiments was to investigate the dependence of the hot melt-bonding performance, in particular, the interleaf penetration depth, on the processing temperature. The melt-bonding temperature was varied between 280 °C and 380 °C. The effect of the interleaf thickness was also considered, with the interleaf thickness varied from 0.005 in. to 0.02 in. This section describes the specimen preparation procedure as well as the employed test and characterization methods.

3.1 Materials and Specimens. The test specimens were fabricated using Saertex 970 g/m^2 glass fiber fabric. The specimens consisted of three core plies of dimensions 11 in. × 1 in., as well as one drop-off ply of dimensions 5.5 in. × 1 in. The drop-off ply was placed on the top of the three core plies, such that the edge of the drop-off ply was located at the center of the specimen. A 2 in. × 1 in. PSU Udel/Thermalux interleaf of a thickness ranging from 0.005 in. to 0.02 in. was inserted between the drop-off ply and the adjacent core ply, such that the edge of the interleaf matched up with the edge of the drop-off ply. The assembly was then clamped between aluminum plates over a length of 2 in. from each side of the drop-off, whereby a uniform pressure of 0.493 MPa was applied. The clamped specimens were then melt bonded in a Carbolite CTF tube furnace at temperatures ranging from 280 °C to 380 °C. The melt-bonded specimens were subsequently processed using the controlled atmospheric pressure resin infusion (CAPRI) method that was patented by the Boeing Corporation (MTS System Corp., Eden Prairie, MN) [24]. The CAPRI process was chosen over the VARTM process since it allowed producing specimens with a higher fiber volume fraction and a lower thickness gradient [25]. The specimens were sealed in a Fibre Glast Stretchlon 800 Bagging Film along with Fibre Glast 582-B Nylon Release Peel Ply (separation media) and Fibre Glast 579-C Breather/Bleeder cloth (distribution media). Once a vacuum was established, the specimens were debulked 75 times by releasing and re-applying the vacuum. Afterward, the epoxy resin was prepared by mixing Momentive Epikote Resin MGS RIMR 135 with Momentive Epikote Curing Agent MGS RIMR 137 at a ratio of 3.39:1. Prior to the infusion, the resin was degasified in a vacuum chamber to remove the excess air that was introduced during mixing. During the infusion, a partial vacuum was maintained at the resin inlet to reduce the pressure gradient between the resin inlet and the vent. Once the entire vacuum bag was infused by the resin, the composite panel was cured at 110 °C for 5 hrs.

3.2 Testing Procedure. The complex interplay of the forces acting inside the turbine blade causes the drop-off plies to be

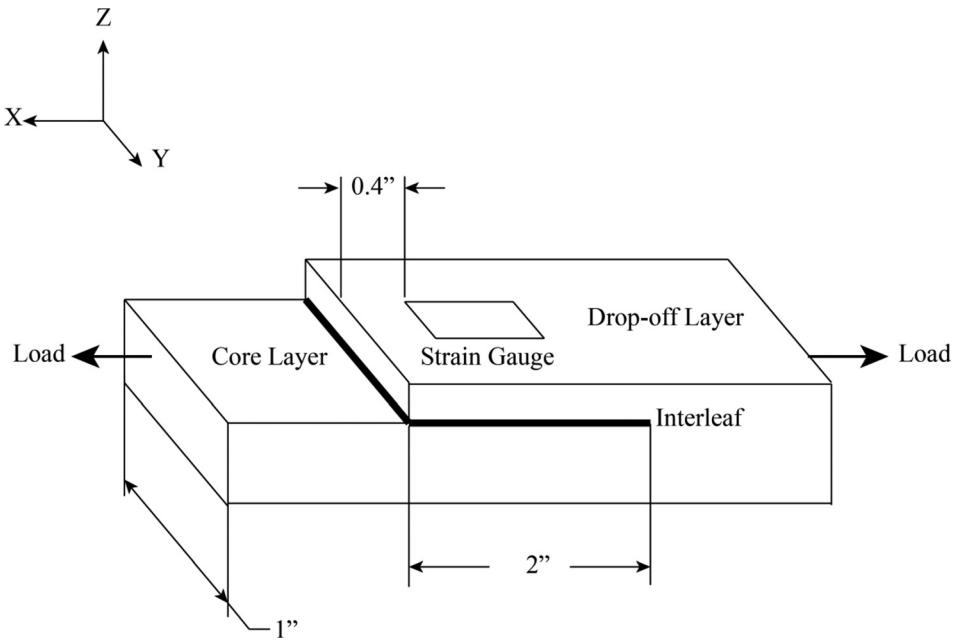

Fig. 5 Three-dimensional schematic diagram describing the mechanical test setup. The strain gauge is placed on the top surface of the external drop-off layer and 0.4 in. away from the edge of the drop-off layer. A 2 in. × 1 in. interleaf is inserted underneath the external drop-off layer and hot melt-bonded before VARTM. Far-field load is in-plane tensile load. Note the coordinate system.

subjected to both normal stresses and shearing stresses, and thus prone to the mixed-mode fracture failure. To simulate the real-life situations, this study employed tensile strength tests as per ASTM-D3039 on an Instron 5569 a universal testing machine. The 11 in. long and 1 in. wide specimens were loaded along the length direction of the specimen as shown in Fig. 5. An Omega 0.6 mm grid and 120 Ω strain gauge was mounted onto the drop-off ply, such that the edge of the strain gauge was at a distance of 0.4 in. from the drop-off. Additionally, the displacements of the core plies were measured using an Instron 2630-103 clip-on strain gauge extensometer. The specimens were loaded until the drop-off layer was entirely delaminated, i.e., until the strain at the strain gauge dropped to zero.

For the post-test analysis, the specimens were cross sectioned along and perpendicular to the length direction. The cross sections were etched by xylene before imaging. An Olympus BX60 differential interference contrast microscope was used to visualize the fracture paths, and a Hitachi S-4700 SEM was used to analyze the fracture surface morphology.

4 Results and Discussion

4.1 Penetration Analysis. Specimens were treated under different temperature conditions with the same pressure. After the hot melt-bonding process, the resin transfer molding was carried out to produce the composites. Each specimen was cut by a diamond saw and the cross section was polished for the optical microscopy.

Figure 6 shows a cross section perpendicular to the drop-off edge, that is, the *Y–Z* plane, and the penetration depth under a lower temperature (280 °C). The gray circles were glass fibers, and the darker area surrounding the fibers was epoxy. The brighter area between the upper and lower plies was the TP interleaf, which penetrated into the fiber bundles. The penetration depth was determined by the color difference observed under optical microscopy. The extent of the penetration is highlighted by curved white lines. As seen, the penetration depth varied from 10 to 60 μm, and the average penetration under this temperature is 32.5 μm.

In comparison, Fig. 7 shows the penetration under a higher temperature (320 °C). The thickness of the interleaf was reduced more and the penetration depth increased significantly. For this case, the penetration of the interleaf ranges from 60 to 150 μm and the average depth is 103.6 μm.

The depth of penetration under temperatures from 280 °C to 380 °C was observed by optical microscopy and calculated by averaging the data from 12 randomly picked locations. The

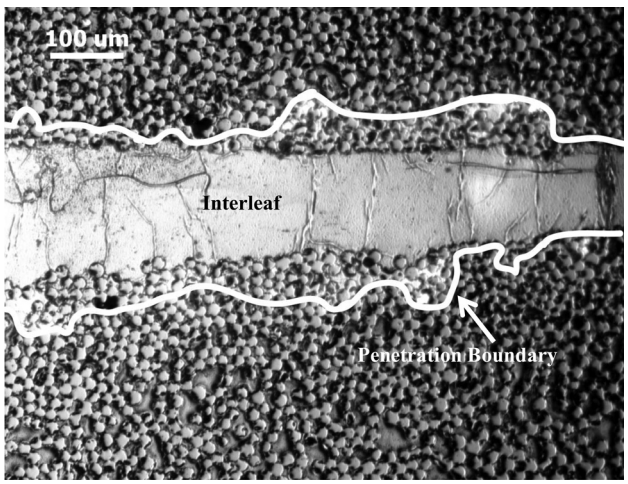

Fig. 6 *Y–Z* cross section (parallel to the drop-off edge) of the specimen with melt-bonded 254 μm thick PSU at 280 °C. Xylene-etched surface shows low penetration of the PSU interleaf into the fiber bundles. Penetration boundary is indicated by the white lines. The average penetration depth is 32.5 μm, and the average remaining interleaf thickness is 168 μm. Due to the low melt-bonding temperature and high viscosity, a limited amount of the interleaf penetrates into the fiber bundles.

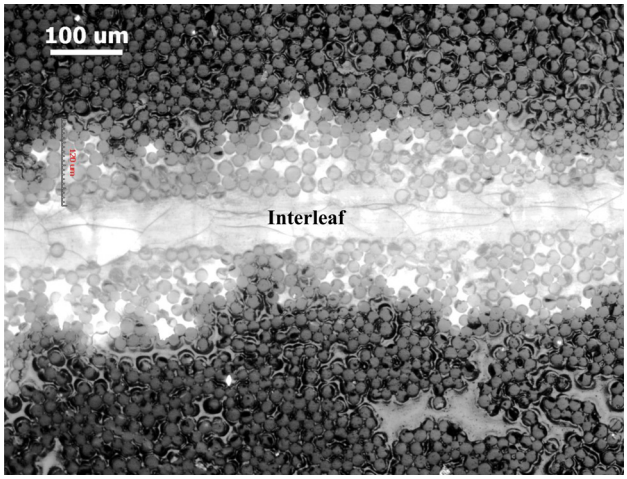

Fig. 7 *Y–Z* cross section of the specimen with melt-bonded 254 μm thick PSU at 320 °C. Xylene-etched surface shows high penetration of the PSU interlayer. The average penetration depth is 103.6 μm, and the average interleaf thickness after melt bonding is 83 μm. Larger penetration depths form a thick mixed region of interlayer and fiber bundles.

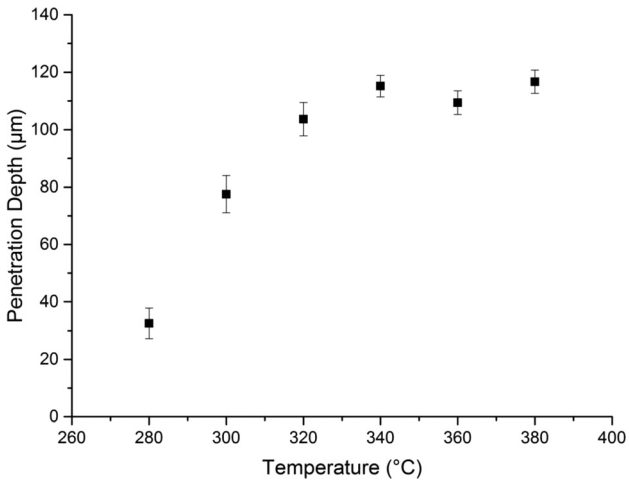

Fig. 8 Experiment results for 254 μm thick PSU interleaf penetration depths from 280 °C to 380 °C. The error bars represent standard errors. The trend of the penetration correlates well with the decreasing viscosity temperature.

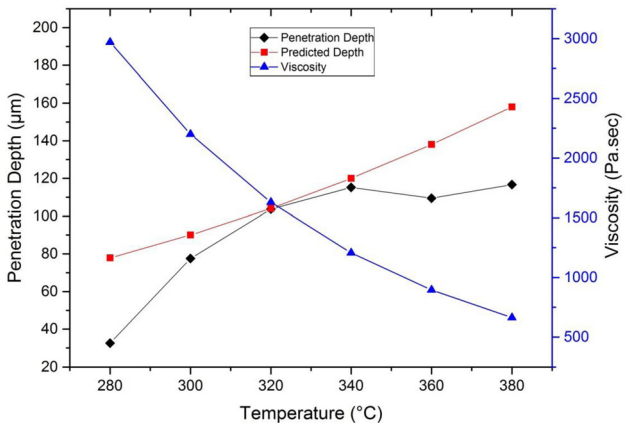

Fig. 9 Predicted and experimental penetration depths increase with the melt-bonding temperature. The trend is primarily due to the deceasing viscosity of the PSU interleaf material with temperature.

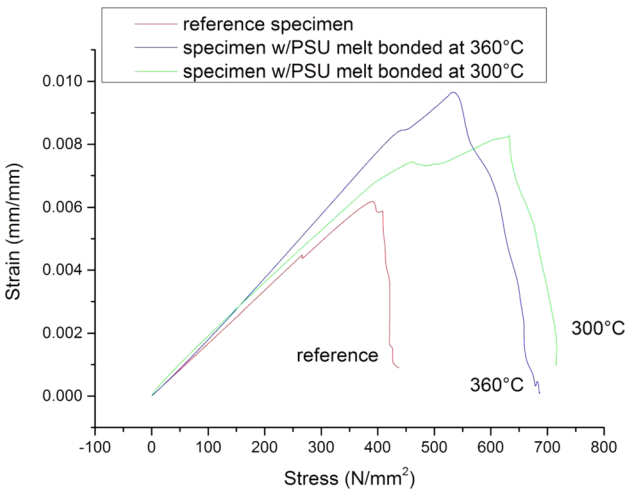

Fig. 10 Representative strain–stress curves obtained from the strain gauge mounted on the drop-off layer in uniaxial tensile tests: reference specimen (without interleaf), interleaved specimens under low/high melt-bonding temperatures. The reference specimen shows the highest stiffness while specimens with interleaf are much tougher.

standard error was calculated to show the variation. From Fig. 8, the penetration depth generally increased with the melt-bonding temperature. The penetration depth rose sharply from 280 °C to 340 °C and leveled off from 340 °C to 380 °C. This is primarily because the viscosity of the PSU TP sharply dropped from 2969 Pa·s at 280 °C to about 1207 Pa·s at 340 °C. The reduction becomes much milder above 340 °C (Fig. 9).

By using the method in Sec. 2, the predicted penetration depths were superposed in Fig. 9 and to compare with the experimental results. Similar to the experimental results, the predicted curve increased with temperature. It, however, overestimated the depth at lower and higher temperatures. The overestimation of the prediction depth at the lower temperature was likely because the model assumed the penetration channels in the porous structure, which have the constant rectangular cross section. In reality, the channel resembles an hourglass in shape. When the temperature was low, the viscosity of the TP interleaf was high and the narrow gap generated greater resistance to the penetration, resulting in higher predicted values. A possible improvement is to model the hourglass shape explicitly. When the temperature was high, the TP interleaf material can penetrate more easily due to the reduced viscosity. However, the thickness reduction of the interleaf was more significant because it was not only related to the penetration depth but also to the flow movement in the *X–Y* plane now, and thus, the assumption that the effect of the applied pressure only depended on the thickness reduction by interleaf penetration likely caused the overestimation at higher temperatures. A possible improvement is to use time- and temperature-dependent pressure.

4.2 Stress–Strain and Toughness Behavior. Uniaxial tensile tests were carried out. The specimens were loaded until the drop-off region was totally delaminated, and thus, the value of the strain gauge returned to zero. Figure 10 shows the stress and strain curves of the drop-off layer under three conditions and they were measured by a strain gauge shown in Fig. 5. The curve marked "reference" referred to the case where no interleaf was introduced. It had the lowest slope among all the curves because the pure epoxy specimen was of higher stiffness. As a result, the reference specimen began to fail at a low strain (about 0.6%). The curves

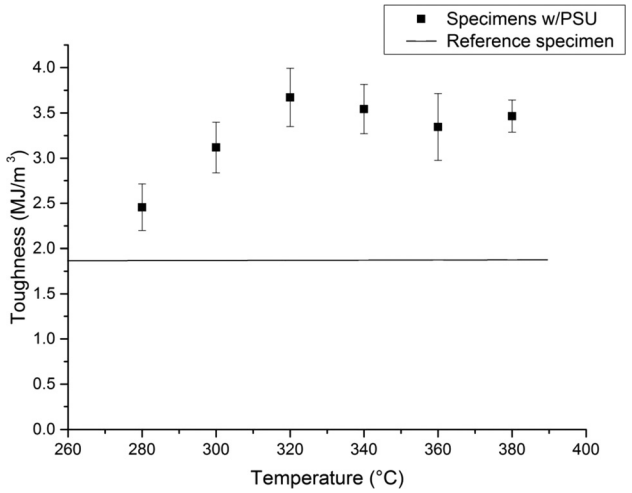

Fig. 11 Toughness of 254 μm thick PSU interleaved specimens from 280 °C to 380 °C. The error bars represent standard errors. The horizontal line represents the average toughness of the specimen without interlayer. The trend correlates well with the trend of the penetration depth (Fig. 8), indicating that the penetration depth directly influences the toughness.

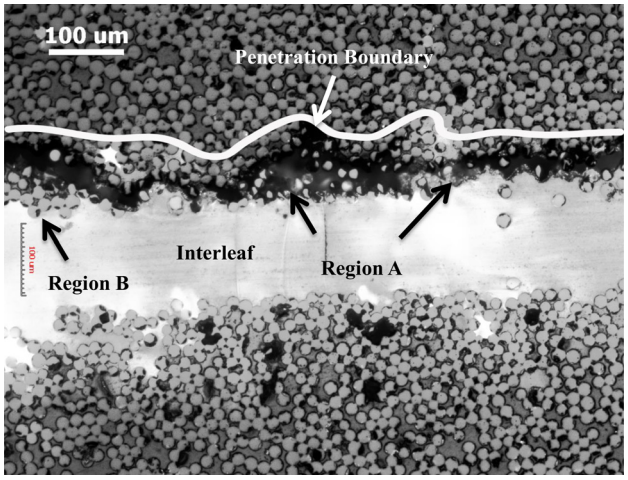

Fig. 12 *Y–Z* cross section (parallel to the drop-off edge) of the fractured specimen with melt-bonded 254 μm thick PSU at 280 °C. The white line indicates the penetration boundary. There are two kinds of the crack locations due to the thin penetration depth. Region A shows that the crack is near the interface between the pure interleaf and the matrix. Region B shows that the crack is near the interface between the interleaf/fiber and epoxy/fiber. The crack reaches the weak interface between interleaf and epoxy under low penetration condition.

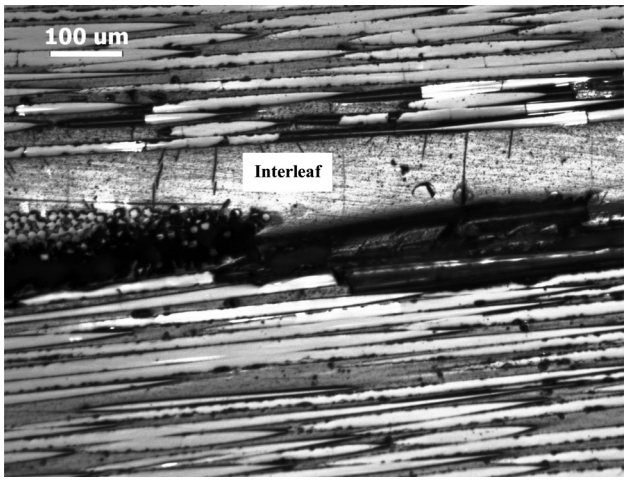

Fig. 13 *X–Z* cross section (perpendicular to the drop-off edge) of the fractured specimen with melt-bonded 254 μm thick PSU at 280 °C. It shows the crack locates at the interface between interleaf and epoxy/fiber or at the interface between interleaf/fiber and epoxy/fiber. Due to the low penetration depth, the crack always propagates along the weak interface between interleaf and epoxy. Less broken fiber, less bridged fiber, and bridged PSU are found compared to the specimen under the high melt-bonding temperature.

whose slopes were higher than the reference specimen were the specimens with melt-bonded interleaf at 300 °C and 360 °C, respectively. As shown in the figure, because of the inserted interleaf, the interlaminar layer connecting the drop-off layer to the core plies became less stiff. For the curve marked 300 °C, it did not fail until the strain reached 0.8% due to its modestly increased penetration depth (Fig. 8). For the curve marked 360 °C, the strain went up about 1% before it began to fail due to markedly increased penetration depth. The reference specimen also showed a sharper drop when it started to fail than the two specimens with interleaf.

The toughness was calculated by integrating the area under the stress–strain curve. It measured the energy required for a crack to initiate and propagate. In Fig. 11, the toughness of reference specimens is represented by a horizontal line. For each melt-bonding temperature, six specimens were tested to validate the data repeatability. Each average toughness and their standard error were represented by a symbol and an error bar. As shown in the figure, the toughness of the specimens had a sharp increase and a peak at the melt-bonding temperature of 320 °C, before it leveled off. The trend resembled that of the penetration depth seen in Fig. 8 and provided strong evidence that deep penetration of the interleaf into the fiber bundles led to the increased toughness, and thus the improved delamination resistance. At its peak, the toughness was almost twice as high as the reference specimen which has no interleaf.

4.3 Crack Path Microscopy. After mechanical tensile tests, all the specimens were cross sectioned and polished to observe the crack morphology. As the crack went into the drop-off region, the crack propagated near the lower interface between interleaf and matrix. Shown in Fig. 12 was the *Y–Z* view of the specimen with 254 μm PSU melt bonded under 280 °C. The dark gully was the crack created after the tensile test. The location of the crack in this figure was mainly located on the interface between the interleaf and the matrix (region A); it was occasionally located inside the fiber bundles where the interleaf penetration is slightly deeper (region B). The *X–Z* view of the crack propagation was shown in Fig. 13. As seen from the image, the crack path was mainly along the interface between resin and interleaf, due to the low melt-bonded temperature, and the penetration depth was only around 30 μm ; as a result, the crack went slightly into the penetration zone (region B) or the interface between interleaf and matrix (region A). In the figure, a few broken fibers were observed, which was another factor leading to the high crack propagation resistance. However, under the low melt-bonding temperature, this kind of broken fibers was not commonly seen.

Figures 14 and 15 show the cross section views of the specimen melt bonded with 254 μm PSU TP interleaf under a higher melt-bonding temperature (320 °C). As shown in the *Y–Z* view in Fig. 14, the crack was located in the region, where the interleaf penetrated into the fiber bundles. Compared with Fig. 12, it was easily observed that the larger penetration depth here, caused by the high melt-bonding temperature, confined the crack entirely within this region, whose toughness has increased due to the

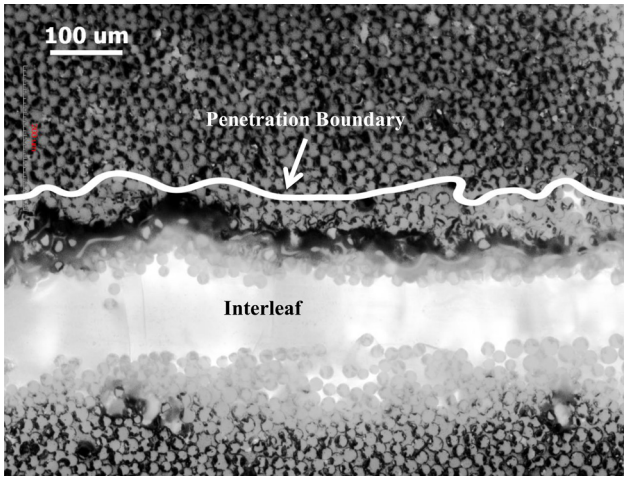

Fig. 14 ***Y–Z*** **cross section of the fractured specimen with melt-bonded 254 μm thick PSU at 320 °C. The white line indicates the penetration boundary. At this melt-bonding temperature, the average penetration depth is 106 μm. The crack propagates through the middle of the penetration region without reaching the weak interface between interleaf and epoxy.**

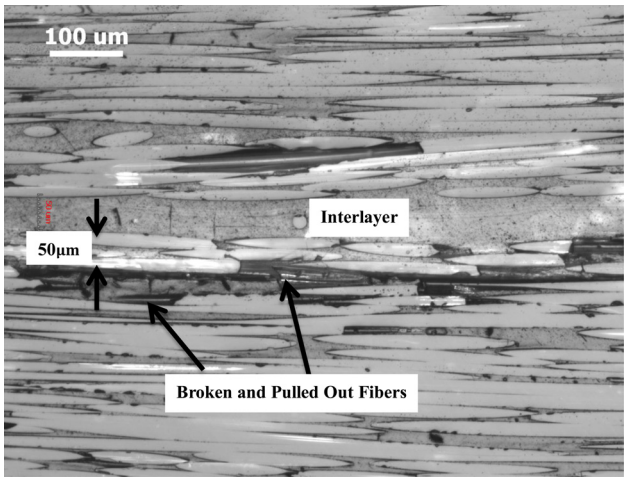

Fig. 15 ***X–Z*** **cross section of the fractured specimen with melt-bonded 254 μm thick PSU at 320 °C. The thickness of the interleaf after the melt bonding reduced to about 63 μm. The crack propagates through the penetration region of interleaf and fibers. The zone is about 106 μm wide as per Fig. 14 under this melt-bonding temperature. More broken fibers and bridged fibers result in high toughness.**

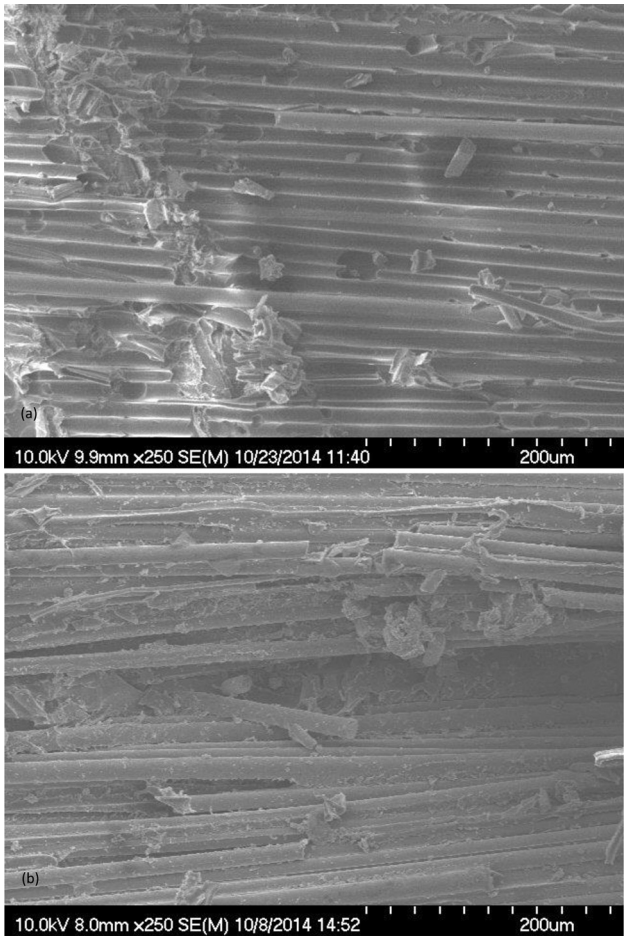

Fig. 16 **(*a*) SEM image of the delamination fracture surface of the specimen with melt-bonded 254 μm thick PSU at 280 °C. The large clean region indicates brittle adhesion failure, which is caused by the crack propagating through the interface between interleaf and epoxy. The rough region indicates the crack goes through the penetration region, where part of the interleaf underwent plastic shear deformation. Fewer broken fibers and pulled-out fibers are found for this condition. (*b*) SEM image for the delamination fracture surface of the specimen with melt-bonded 254 μm thick PSU at 320 °C. The much rougher surface indicates more ductile fracture has taken place. Plastic shear deformation of the interleaf can be seen around fiber beams. More broken fibers and pulled-out fibers are seen for this condition due to the increased delamination resistance.**

penetrated TP interleaf. From Fig. 15, the *X–Z* plane image also indicated that the crack propagated not through the interface between the interleaf and fiber bundles. As the penetration depth under 320 °C was 106 μm, the crack resided around the central part of the penetration region. Contrary to Fig. 13, Fig. 15 showed more broken fiber beams and more bridged fibers pulled out from the matrix, which led to a higher delamination resistance.

These results confirmed our hypothesis indicated in Fig. 3. When the interleaf penetration was low, the plastic zone ahead the crack tip was more likely to reach the interface of the interleaf and the epoxy. As the stiffness of the epoxy was higher than that of the TP interleaf, one did not benefit from the full plastic zone, which absorbed more energy, as part of the zone cannot develop within the epoxy zone (Fig. 3(*a*)). When the penetration depth was high, as the strength of the interface between the PSU interleaf and penetration region was still lower than the stress ahead of the crack tip, the crack also went to the penetration region; however, it is more likely to remain within the region as it is larger now (Fig. 3(*b*)). As a result, the penetration region localized and arrested the crack, and the high toughness of the penetration region required more energy for the crack to propagate.

4.4 Fracture Surface Morphology. Fracture surfaces of the specimens after mechanical tensile tests were observed via SEM. Figure 16(*a*) shows the typical fracture surface of the specimen with 254 μm thick interleaf melt bonded at 280 °C. From the figure, it showed two kinds of fracture surface. The first kind was clean where fewer broken fiber beams were found on the surface: individual fiber beam was seen with very few particles on its surface; clean and clear river lines between the fibers indicated that there was no plastic shear deformation; and fewer pulled-out fibers were found on this type of surface. It was obvious that this fracture surface was the interface between interleaf and fiber or between epoxy and fiber, which was the weak region in the structure and led to the low fracture toughness. The other kind showed rougher surface: the brighter lumps showed large shear

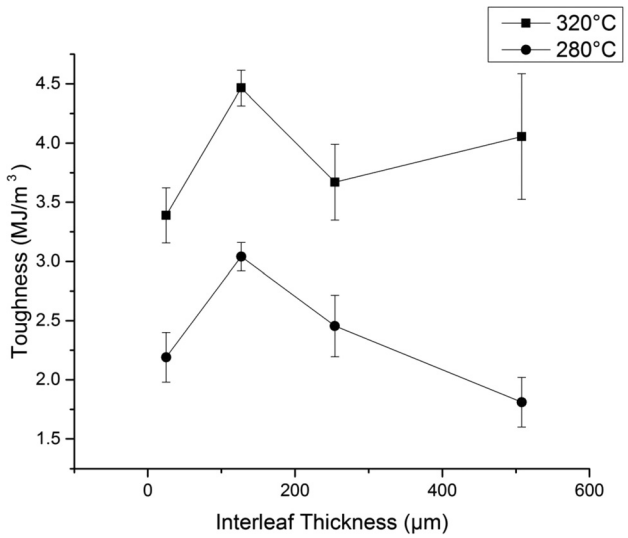

Fig. 17 Toughness of the specimens versus interleaf thickness under different melt-bonding temperatures. The error bars represent standard errors. The sharp increasing toughness from 25 μm to 127 μm is due to more participated TP interleaf in plastic deformation. After the peak point, the toughness decreases with interleaf thickness. It is because the influence of the mismatch of the drop-off structure and materials is magnified and induces adhesive failure, which reduces the toughness. For the specimens melt bonded at the higher temperature, which has a higher penetration depth and thus the better bonding quality, some toughness is preserved even the interleaf gets overly thick.

deformation, which improved the toughness; however, there was not much torn interleaf remaining on the surface. The crack of both kinds mainly went through the interface between interleaf and fiber or epoxy and fiber, which led to adhesive failure. For the PSU interleaved specimen melt bonded at 320°C (Fig. 16(*b*)), more broken fibers and pulled-out fibers were observed throughout the fracture surface. Most debonded fibers were not clean with small particles or lumps of the "torn resin" attached on the fiber, which indicated large plastic deformation. Because of the high penetration depth, the mixed region with fiber beams, TP, and thermoset resin was deep into the fiber matrix, which led to the phenomenon that even the fibers below the contact interface between TP and fiber bundles were also pulled out from the matrix. More participated pulled-out fibers and broken fibers directly increased the toughness and thus delamination resistance. The present results indicated that high toughness interleaf and high penetration into the fiber bundles were both the key factors to improve the toughness of the composites, avoid the adhesion failure, and enhance the bonding quality.

4.5 Influence of Interlayer Thickness. The thickness of interlayer may influence the toughness of the specimens. The specimens with interlayer thickness from 25 μm to 508 μm were tested under two different temperatures (280 °C and 320 °C) to investigate the crack resistance behavior. As shown in Fig. 17, under the lower melt-bonding temperature, the toughness of the specimen had a significant increasing when the interlayer thickness increased from 25 μm to 127 μm. However, it decreased after 127 μm. The low toughness with the 25 μm thick interleaf was likely due to the inadequately participated interleaf in plastic deformation because the interleaf was thin. When the thickness increased to 127 μm, the toughness increased. But when the thickness increased further, the influence of stress concentration could be magnified [26], and thus the toughness reduced. Under the higher melt-bonding temperature (320 °C), the trend was similar except with thicker interleafs, and the toughness reduction was not as pronounced. This was likely due to the fact that the interlayer went deeper into the fiber bundles to offset the stress concentration effect mentioned above.

5 Conclusion

The effect of the interleaf deep penetration on the mixed-mode delamination resistance was investigated for the PSU TP interleaved GFRP. The penetration depth increased with the hot-melting bonding temperature to a certain value and then leveled off. This is mainly due to the PSU viscosity behavior, which decreases quickly to around that value and then decreases slowly. As compared with the GFRP without interleaf, the fracture toughness increased by a factor of two with the penetration depth of the 254 μm PSU TP interleaf into the fiber bundles reached 100 μm under melt-bonding temperature of 320 °C, and increased 2.5 times with 127 μm PSU TP interleaf under melt-bonding temperature of 320 °C. This is mainly because the deep penetration zone of improved ductility confines the plastic zone ahead of the crack tip within its boundaries, and thus requires more facture energy for the crack to propagate. Pulled-out and broken fibers were also responsible for the increased toughness. In the case where the penetration is shallow, the plastic zone is likely to reach the interface of the interleaf of the epoxy matrix, and thus, the benefit of increase toughness due to interleafing cannot be fully realized.

Acknowledgment

This research was supported by National Science Foundation under Award No. CMMI-1363328. The authors also would like to thank Paul Ubrich from Momentive Specialty Chemicals, Inc., for providing experiment materials.

References

[1] Leach, D. C., and Moore, D. R., 1985, "Toughness of Aromatic Polymer Composites Reinforced With Carbon Fibers," Compos. Sci. Technol., **23**(2), pp. 131–161.
[2] Takashi, I., and Masamichi, M., 1997, "Compression After Impact (CAI) Properties of Hat Stiffened CF/PEEK Panels Fabricated Through a Route Without Autoclave," ICCM-11, Gold Coast, Australia, July 14–17, pp. 1–9.
[3] Cairns, D. S., Mandell, J. F., Scott, M. E., and Maccagnano, J. Z., 1999, "Design and Manufacturing Considerations for Ply Drops in Composite Structures," Compos. Part B: Eng., **30**(5), pp. 523–534.
[4] Ozdil, F., and Carlsson, L. A., 1992, "Mode I Interlaminar Fracture of Interleaved Graphite/Epoxy," J. Compos. Mater., **26**(3), pp. 433–459.
[5] Groleau, M. R., Shi, Y. B., Yee, A. F., Bertram, J. L., Sue, H. J., and Yang, P. C., 1996, "Mode II Fracture of Composites Interleafed With Nylon Particles," Compos. Sci. Technol., **56**(11), pp. 1223–1240.
[6] Hillermeier, R. W., and Sefeis, J. C., 2001, "Interleaf Toughening of Resin Transfer Molding Composites," Compos.: Part A, **32**(5), pp. 721–729.
[7] Li, G., Li, P., Zhang, C., Yu, Y. H., Liu, H. Y., Zhang, S., Jia, X. L., Yang, X. P., Xue, Z. M., and Ryu, S. K., 2008, "Inhomogeneous Toughening of Carbon Fiber/Epoxy Composite Using Electrospun Polysulfone Nanofibrous Membranes by in Situ Phase Separation," Compos. Sci. Technol., **68**(3–4), pp. 987–994.
[8] Magniez, K., Chaffraix, T., and Fox, B., 2011, "Toughening of a Carbon-Fibre Composite Using Electrospun Poly(Hydroxyether of Bisphenol A) Nanofibrous Membranes Through Inverse Phase Separation and Inter-Domain Etherification," Materials, **4**(12), pp. 1967–1984.
[9] Zhang, J., Yang, T., Lin, T., and Wang, C. H., 2012, "Phase Morphology of Nanofibre Interleafs: Critical Factor for Toughening Carbon/Epoxy Composites," Compos. Sci. Technol., **72**(2), pp. 256–262.
[10] Wu, X. F., Rahman, A., Zhou, Z. P., Pelot, D. D., Sinha-Ray, S., Chen, B., Payne, S., and Yarin, A. L., 2012, "Electrospinning Core-Shell Nanofibers for Interfacial Toughening and Self-Healing of Carbon-Fiber/Epoxy Composites," J. Appl. Polym. Sci., **129**(3), pp. 1383–1393.
[11] Kuwata, W., and Hogg, P. J., 2011, "Interlaminar Toughness of Interleaved CFRP Using Non-Woven Veils," Compos.: Part A, **42**(10), pp. 1551–1570.
[12] Matsuda, S., Hojo, M., Ochiai, S. A., Murakami, Akimoto, H., and Ando, M., 1999, "Effect of Ionomer Thickness on Mode I Interlaminar Fracture Toughness for Ionomer Toughened CFRP," Compos. Part A, **30**(11), pp. 1311–1319.
[13] Hojo, M., Matsuda, S., Tanaka, M., Ochiai, S., and Murakami, A., 2006, "Mode I Delamination Fatigue Properties of Interleaf-Toughened CF/Epoxy Laminates," Compos. Sci. Technol., **66**(5), pp. 665–675.
[14] Hojo, M., Matsuda, S., Ochiai, S., Marukami, A., and Akimoto, H., "The Role of Interleaf/Base Lamina Interphase in Toughening Mechanism of Interleaf-Toughened CFRP," ICCM-12 Conference, Paris, p. 410.

[15] Jensen, F. M., Falzon, B. G., Ankersen, J., and Stang, H., 2006, "Structural Testing and Numerical Simulation of a 34m Composite Wind Turbine Blade," Compos. Struct., **76**(1–2), pp. 52–61.
[16] 2010, "Upsizing Blade Test Regimes," Composites Technology, Last accessed Sept. 15, 2015.
[17] Shim, D. J., and Lagace, P. A., 2006, "Mechanisms and Structural Parameters Affecting the Interlaminar Stress Field in Laminates With Ply Drop-Offs," J. Compos. Mater., **40**(11), pp. 345–369.
[18] Shim, D. J., 2002, "Role of Delamination and Interlaminar Fatigue in the Failure of Laminates With Ply Dropoffs," Ph.D. thesis, Massachusetts Institute of Technology, Boston, MA.
[19] Chen, S. F., and Zhang, B. Z., 1991, "Fracture Behavior of Interleaved Fiber-Resin Composites," Compos. Sci. Technol., **41**(1), pp. 77–97.
[20] Brewer, J. C., and Lagace, P. A., 1988, "Quadratic Stress Criterion for Initiation of Delamination," J. Compos. Mater., **22**(12), pp. 1141–1155.
[21] Aksoy, A., and Carlsson, L. A., 1991, "Crack Tip Yield Zone Estimates in Mode II Interlaminar Fracture of Interleaved Composites," Eng. Fract. Mech., **39**(3), pp. 525–534.
[22] Smiley, A. J., Chao, M., and Gillespie, J. W., 1991, "Influence and Control of Bondline Thickness in Fusion Bonded Joints of Thermoplastic Composites," Compos. Manuf., **2**(3–4), pp. 223–231.
[23] SolvayPlastic, Udel@PSU Design Guide, p. 55.
[24] Woods, J., Modin, A. E., Hawkins, R. D., and Hanks, D. J., 2002, "Controlled Atmospheric Pressure Infusion Process," International Patent WO 03/101708 A1.
[25] Niggemann, C., Young, S. S., Gillespie, J. W., and Heider, D., 2008, "Experimental Investigation of the Controlled Atmospheric Pressure Resin Infusion (CAPRI) Process," J. Compos. Mater., **42**(11), pp. 1049–1061.
[26] Mandell, J. F., Samborsky, D. D., Agastra, P., Sears, A. T., and Wilson, T. J., 2010, "Analysis of SNL/MSU/DOE Fatigue Database Trends for Wind Turbine Blade Materials," Contractor Report No. SAND2010-7052, Sandia National Laboratories, Contractor Report No. SAND2010-7052.